View metadata, citation and similar papers at core.ac.uk
brought to you by CORE
provided by CERN Document Server

Anomalies in the Nuclear Dissociation Cross Sections of ^{208}Pb at 33 TeV

S. Datz,[1] J. R. Beene,[1] P. Grafström,[2] H. Knudsen,[3] H. F. Krause,[1] R. H. Schuch,[4] and C. R. Vane[1]
[1]*Physics Division, Oak Ridge National Laboratory, P.O. Box 2008, Oak Ridge, Tennessee 37831-6377*
[2]*CERN, SPS/SL Division, Batiment 866, CH-1211, Geneva 23, Switzerland*
[3]*Institute of Physics and Astronomy, Aarhus University, DK-8000, Aarhus C, Denmark*
[4]*Atomic Physics Department, Stockholm University, Frescativägen 24, S-104 05, Stockholm, Sweden*
(Received 24 February 1997)

We have measured total nuclear disintegration cross sections for ^{208}Pb ions at 33 TeV (160-GeV A) colliding with C, Si, Cu, Sn, and Pb. Using well established theory, we calculate the nuclear electromagnetic, electron electromagnetic, and the hadronic contributions and find that their sum underestimates the measured cross sections. An additive correction term linear in target Z_T (i.e., $120Z_T$ mb) is necessary to bring agreement between theory and experiment. The source of this additional term is unknown. [S0031-9007(97)04384-6]

PACS numbers: 25.75.–q, 24.30.Cz

Dissociation of relativistic heavy ions (RHI) by the electromagnetic field of target nuclei has been studied extensively for two decades [1–5]. Recent experimental work has concentrated on efforts to isolate the effects of multiple excitations of the giant dipole resonance (multiphonon excitations) in experimental dissociation data [6–9]. Plans for the construction of RHI colliders at Brookhaven and CERN have, however, generated renewed interest in the very large total dissociation cross sections expected for ultrarelativistic heavy ions [10], since these processes can be important mechanisms for beam loss in such machines [10–12].

In almost all experimental studies of electromagnetic dissociation to date, the yields of particular residual nuclei are determined which result from the decay of the beam nuclei subsequent to the primary beam-target interaction. In order to relate these data to the cross section for the primary process, it is necessary to employ models which account in detail for both the excitation and decay processes. In this paper, we report a direct measurement of the total projectile dissociation cross section, with no need for modeling of excited projectile decay.

Even though electromagnetic processes occurring at a large impact parameter dominate the dissociation cross section of relativistic energies, hadronic processes resulting from more central collisions remain significant even for ultrarelativistic beams. Fortunately, the two mechanisms can be disentangled to a large extent by making use of the very different dependence they show on the Z of the target nucleus, for a given projectile species and energy. In this Letter, we report measurements on the dissociation of ^{208}Pb nuclei at 33 TeV in targets of C, Si, Cu, Sn, and Pb.

Electromagnetic processes at relativistic and ultrarelativistic energies can be treated accurately using the equivalent photon method [12–16]. The cross section for excitation of a projectile by the electromagnetic pulse it experiences is obtained by folding the photoabsorption cross section $\sigma_\gamma(E_\gamma)$ of the projectile with the equivalent virtual photon spectrum $n(E_\gamma)$ seen by the projectile as it passes the target. The calculation of $n(E_\gamma)$ requires an integration over the impact parameter b of the collision; for impact parameters less than some minimum value $b_{\min}$, hadronic processes dominate. Consequently, impact parameters less than $b_{\min}$ are excluded from the electromagnetic calculation. This leads to a rough upper limit to the energies in the virtual photon spectrum, and hence to excitation energies which can be reached by electromagnetic processes, given by [16]

$$E_\lambda^{\max} = \frac{\gamma_p \hbar c}{b_{\min}}, \tag{1}$$

where γ_p is the Lorentz boost parameter of the projectile motion relative to the target nucleus. For a 33-TeV ^{208}Pb beam incident on the five targets in this study, $E_\gamma^{\max}$ ranges from 2.1 GeV for Pb to 3.2 GeV for carbon. The equivalent photon number spectra $n_{\pi\lambda}$ depend on the electric or magnetic character ($\pi = E$ or M) and the multipolarity λ as well as the energy. At low collision energies ($\gamma_p \sim 1$), higher multipolarity photons are much more plentiful than dipole photons, so that quadrupole excitation often dominates. For $\gamma_p \gg 1$, the $n_{\pi\lambda}$ converge to the same value n. Our data are at sufficiently high energy ($\gamma_p \sim 170$) that our calculations ignored the multipolarity dependence of $n_{\pi\lambda}$. Subsequent checks using the explicitly $\pi\lambda$ dependent expression (Eq. 2.5.4 from Ref. [16]), show that a small ($\sim$3%) correction is necessary for the excitation of the giant quadrupole resonances at 10 MeV (isoscalar) and 22 MeV (isovector) in ^{208}Pb.

Our calculation requires photoabsorption cross sections for photon energies up to $E_\gamma \sim 3$ GeV. We employed $\sigma_\gamma(E_\gamma)$ taken from experimental results for ^{208}Pb up to $E_\gamma \sim 500$ MeV [17–20]. For higher energies, we used the experimental proton total cross section [21], $\sigma_{\gamma p}$,

 © 1997 The American Physical Society

scaled by the mass number A [12,17]; i.e., $\sigma_\gamma(E_\gamma) \approx 208\sigma_{\gamma p}(E_\gamma)$. This hybrid σ_γ for ^{208}Pb is illustrated in Fig. 1. A shadowing correction is sometimes applied in relating σ_γ to $\sigma_{\gamma p}$. Shadowing is certainly important above about $E_\gamma \sim 4$ GeV [17], but probably plays a negligible role at the energies relevant to this calculation [17].

The total electromagnetic (EM) dissociation cross section is therefore [16]

$$\sigma_{\mathrm{EM}} = \int_{S_n}^{\infty} \frac{n(E_\gamma)\sigma_\gamma(E_\gamma)}{E_\gamma}\, dE_\gamma\,, \qquad (2)$$

where S_n is the lowest particle emission threshold (the neutron separation energy in Pb). The σ_{EM} calculated for ^{208}Pb from Eq. (2) for the conditions appropriate to our experiment is dominated by the giant dipole resonance (GDR) at an excitation energy of $\sim$13.5 MeV (see Fig. 1). For purposes of illustration, we divided the calculation of σ_{EM} into three energy regions: S_n–30 MeV (GDR region), 30–500 MeV (quasideuteron plus nucleon excitation region), and 500–2500 MeV. For the five targets considered, $\sim$82%–85% of σ_{EM} is accounted for by the GDR region (excitation energy 7.4 to 30 MeV), $\sim$13%–15% of σ_{EM} by the 30 to 500 MeV region, and $\sim$2%–3% of σ_{EM} by energies above 500 MeV. If the interacting nuclei were point objects ($b_{\mathrm{min}} = 0$), the cross section for single virtual photon absorption would vary with target Z as Z^2. The finite b_{min} introduces an additional nuclear size dependence correlated with Z that reduces the effective exponent of Z by an amount that increases with the energy of the virtual photon exchanged. In the GDR region, the effective exponent is 1.96, falling to 1.85 above 600 MeV. Since the total calculated cross section is dominated by GDR excitation, σ_{EM} scales as $\sim Z_T^{1.95}$.

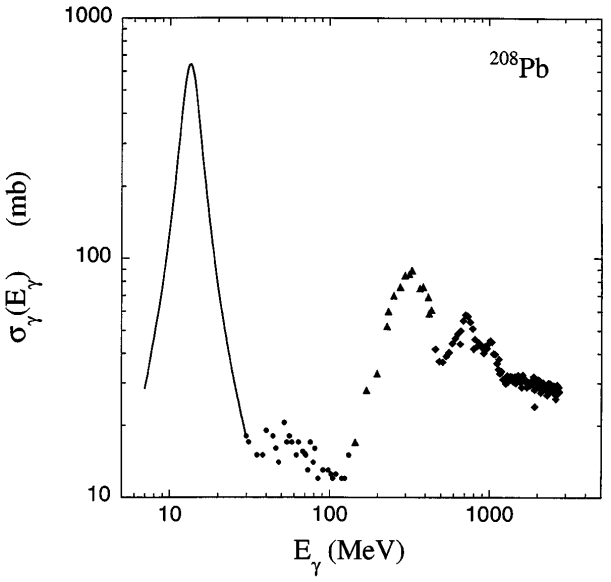

FIG. 1. The solid line is a Lorentzian fit to data in Ref. [18], the circles are from Ref. [19], the triangles are from Ref. [20], and the diamonds are scaled proton data from Ref. [21].

The formalism outlined above leads to very large excitation probabilities, especially for impact parameters just above b_{min}; in fact, it has been pointed out [12,16] that straightforward application of the equivalent photon method can lead to excitation probabilities in excess of the unitarity limit for small b. We have used a method [12,16] based on the harmonic oscillator approximation [12,16] to correct for this effect. For simplicity, we applied the correction to impact parameters from b_{min} to 50 fm for all five systems, and performed the standard calculation for $b > 50$ fm. The correction is negligible for targets lighter than Sn, but reduces the cross section by 2.2% for Pb + Sn and by 4.6% for Pb + Pb. The calculated values for σ_{EM} are listed in column (a) of Table I. The uncertainties in the calculation of the electromagnetic cross section are dominated by the uncertainty in the photoabsorption cross sections. We estimate an overall uncertainty of $\sim$8% in the electromagnetic calculation. The treatment of the unitarity problem is based on the harmonic oscillator approximation which is probably accurate to about 10% in this context, but since the total correction due to this effect is so small, no significant additional contribution to the uncertainty in the calculation results.

Hadronic processes account for a significant part of the total projectile dissociation cross section, even for Pb + Pb at $\gamma_p \approx 170$. Detailed systematics are available for total hadronic reaction cross sections (σ_h) of heavy ions at low energies [22]. Extrapolated to high energies where the Coulomb barrier is negligible compared to the bombarding energy, these low energy systematics give a geometrical cross section $\sigma_h = \pi R_{\mathrm{int}}^2$, where R_{int}, the interaction radius, is, roughly speaking, the sum of the radii of the reactant nuclei. The parametrizations [22] of R_{int} obtained from fitting low-energy data are not adequate for high energies. If we represent the high-energy total nuclear cross section by $\sigma_h = \pi b_c^2$, where b_c represents the critical impact parameter beyond which inelastic excitations due to hadronic interactions do not occur, we find that $b_c < R_{\mathrm{int}}$, reflecting the transparency effect in nucleus-nucleus collisions at high energies. The Glauber [23] framework has been used to deal quantitatively with transparency, and provide reliable estimates of σ_h in terms of nuclear density distributions and total nucleon-nucleon cross sections [24–26]. We employ one such Glauber-type approach, the soft spheres model of Karol [25], using a droplet model expression to relate the radius parameter of the nuclear density distribution to A and Z [27], and $\sigma_{NN} =$ 39 mb [21] (appropriate to 160 GeV nucleon scattering). It is interesting to consider the ratio of the b_c deduced from the soft-spheres model to the R_{int} from the low-energy systematics: This ratio increases smoothly with the increasing sum of the mass number of the projectile and target, ranging from 0.87 for C + Pb to 0.99 for

TABLE I. Theoretical and experimental cross sections (in barns) for processes contributing to the dissociation of 160-GeV A ^{208}Pb ions as a function of target Z_T.

Z_T	A	σ_{EM} (a)	σ_e (b)	σ_h (c)	Total theory (d)	Theory+ $0.12Z_T$ (e)	Total Experiment (f)
6	12	0.282	0.051	3.423	3.763	4.5	4.5
14	28	1.501	0.133	4.342	5.976	7.6	7.4
29	63	6.229	0.275	5.473	11.978	15.4	15.2
50	120	17.807	0.475	6.609	24.924	30.9	31.0
82	208	45.62	0.779	7.856	54.259	64.1	64.0

Pb + Pb. The quantity b_c deduced from σ_h was used in our calculations for the parameter $b_{\min}$ in the electromagnetic calculations. The calculated values of σ_h are listed in column (b) of Table I.

Finally, consider the contribution of the electrons bound to the target nuclei, σ_e. The kinematics of the reaction are equivalent to bombardment of a stationary Pb nucleus by 86-MeV electrons. A calculation of the electrodisintegration cross section of ^{208}Pb by 86-MeV electrons using the same methods as for nuclear EM excitation [16] gives a value of 9.5 mb per electron. The values of σ_e are listed in column (c) of Table I.

The experimental setup has been described previously [27]. The $^{208}Pb^{82+}$ beam at 33 TeV is delivered from the CERN SPS accelerator and is monitored by secondary emission detectors made from thin foils placed in the way of the beam. It is then bent 42 mrad by an array of dipoles, it is collimated by a set of slits, and is momentum analyzed using a collimator slit $\sim$150 m downstream. After a passage of $\sim$300 m, it is bent again and focused onto a detector $\sim$350 m further downstream. The detector used was a fast Cherenkov counter. The slits are $\sim$1 m thick; they can be set to a width as low as 2 mm and can be moved in 2 mm steps. The momentum calibration can either be calculated from the beam optics or it can be experimentally determined from the positions registered for ^{208}Pb and ^{207}Pb in a single scan of the slits. The latter is copiously formed by neutron stripping in all targets. The measured resolution of the system is $\sim 7 \times 10^{-4}$ which permits the location of a peak to be determined with a precision of 1×10^{-4}. The targets are mounted on a ladder in two parallel arrays that can be moved vertically and horizontally for positioning. Because the ladder is located almost 1 km from the control room in an inaccessible and high radiation area, a special personal computer control and data acquisition system was created and is described elsewhere [28]. Four targets of each element were mounted on the ladder. The attenuations were determined by integration of the transmitted beam intensities and ranged from, e.g., 0.69 to 0.08 for carbon and 0.53 to 0.015 for Pb. An example (e.g., Si) is shown in Fig. 2. The beam was broadened by multiple Coulomb scattering (MCS) and, in some cases, was partially cut by the collimator slits set at $\pm$2 mm 30 m downstream. The MCS scattering widths transmitted through the system were measured and shown to conform to expectations [26]. A Monte Carlo calculation from the beam optics showed that the clipping due to MCS was small except in the case of the thick Pb targets. These effects are taken into account in our calculations. The error limits derive from two sources. The largest contribution comes from an uncertainty in the beam monitor calibration versus the Cherenkov counter as it enters into the measured beam profile intensity. From twenty separate scans made with open beam during the run, we obtained a relation between the beam monitor and the Cherenkov detector that was constant to $\sim$10%. The average deviation of experimental points from an exponential decay fit ($\pm$5%) added in quadrature for each element gives an absolute error estimate $\sim\pm$11%.

The total experimental cross sections for the five systems are listed in column (f) of Table I and are shown in Fig. 3, along with calculated hadronic and electromagnetic cross sections, and the calculated total cross section. The very different Z_T dependencies of σ_{EM} and σ_h are evident, as is the fact that the calculations give a total cross section significantly less than the measured one. To try to locate the source of this discrepancy,

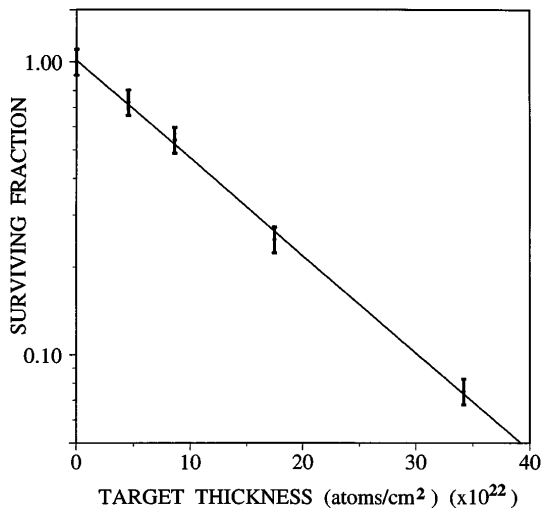

FIG. 2. Attenuation of 160-GeV A ^{208}Pb in the silicon target as a function of target thickness in units of 10^{22} atoms/cm^2.

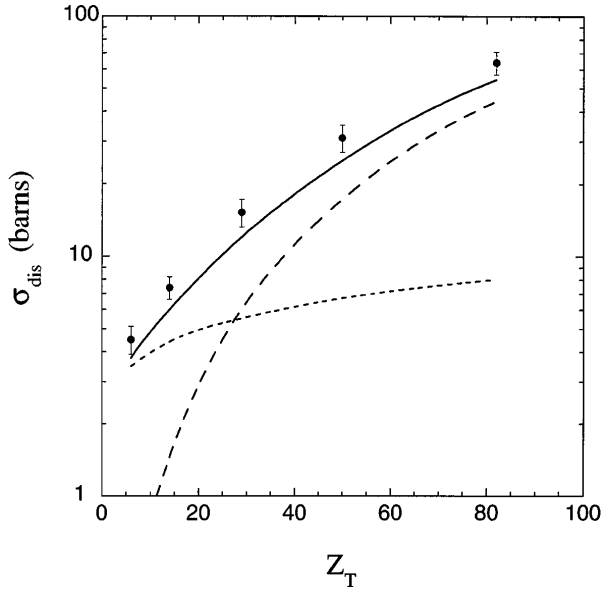

FIG. 3. Experimental dissociation cross sections and calculated hadronic, electromagnetic, electronic, and total cross sections.

we assume that two of the three components of the calculated cross sections are correct, subtract them from the experimental data, and thereby attempt to isolate a hypothetical anomalous cross section.

First we subtract the calculated σ_{EM} and σ_e contributions and consider that the correction lies in the hadronic cross section. We find that $1.43\sigma_h$(calc) fits the data reasonably well. However, this would imply a critical impact parameter $b_c \sim 20\%$ larger than calculated and, for heavy systems, significantly larger than R_{int}. This is not plausible.

If we isolate the EM cross section, we find an equally unlikely situation. A scaled theoretical EM cross section does not fit the data, and rather than following the anticipated Z_T^2 scaling, the "isolated" experimental EM cross sections scale as $Z_T^{1.68}$.

Finally, if we ascribe the discrepancy to the electronic term, i.e., a term that is linear with Z_T, remarkably good agreement is obtained by inserting an *additive* term of Z_T (0.13 ± 0.03 b), i.e., 130 mb per electron. This adduced electron induced excitation cross section is an order of magnitude larger than the accepted value of 9.5 mb. The result of adding the difference ($0.12Z_T$ b) shown in column (e) of Table I gives excellent agreement well within the stated error over the entire range of Z_T. However, the source of this term is not understood.

Authors S.D., H.F.K., and C.R.V. acknowledge the support of the U.S. Department of Energy, Office of Basic Energy Sciences, Division of Chemical Sciences, and J.R.B. acknowledges support of the Office of Energy Research, Division of Nuclear Physics. Both programs are under Contract No. DE-AC05-96OR22464 with Lockheed Martin Energy Research Corporation. H. K. acknowledges the support of the Danish Natural Science Research Council.

[1] H. H. Heckman and P. J. Lindstrom, Phys. Rev. Lett. **37**, 56 (1976).
[2] D. L. Olson *et al.*, Phys. Rev. C **24**, 1529 (1981).
[3] M. T. Mercier *et al.*, Phys. Rev. Lett. **52**, 898 (1984).
[4] M. T. Mercier *et al.*, Phys. Rev. C **33**, 1655 (1986).
[5] W. J. Llope and P. Braun-Munziger, Phys. Rev. C **41**, 2644 (1990).
[6] W. J. Llope and P. Braun-Munziger, Phys. Rev. C **45**, 799 (1992).
[7] T. Aumann *et al.*, Phys. Rev. C **47**, 1728 (1993).
[8] T. Aumann *et al.*, Z. Phys. A **352**, 163 (1995).
[9] H. Emling, Prog. Part. Nucl. Phys. **33**, 729 (1994), and references therein.
[10] G. Baur and C. A. Bertulani, Nucl. Phys. **A505**, 835 (1989).
[11] D. Brandt, K. Eggert, and A. Morsch, CERN LHC Report No. 264, 1994.
[12] A. J. Baltz, M. J. Rhodes Brown, and J. Weneser, Phys. Rev. E **54**, 4233 (1996).
[13] E. Fermi, Z. Phys. **29**, 315 (1924).
[14] C. F. Weiszaecker, Z. Phys. **88**, 612 (1934).
[15] E. J. Williams, Phys. Rev. **45**, 729 (1934).
[16] C. A. Bertulani and G. Baur, Nucl. Phys. **A442**, 739 (1985); C. A. Bertulani and G. Baur, Phys. Rep. **163**, 299 (1988).
[17] J. Ahrens, Nucl. Phys. **A446**, 229 (1985).
[18] A. Veyssiere *et al.*, Nucl. Phys. **A159**, 561 (1970).
[19] A. Lepretre *et al.*, Nucl. Phys. **A367**, 237 (1981).
[20] P. Carlos *et al.*, Nucl. Phys. **A431**, 573 (1984).
[21] Particle Data Group, R. M. Barnett *et al.*, Phys. Rev. D **54**, 1 (1996).
[22] W. W. Wilke, At. Data Nucl. Data Tables **25**, 389 (1980).
[23] R. J. Glauber, in *High Energy Physics and Nuclear Structure*, edited by G. Alexander (North-Holland, Amsterdam, 1967), p. 311.
[24] C. J. Benesh, B. C. Cook, and J. P. Vary, Phys. Rev. C **40**, 1198 (1989).
[25] P. J. Karol, Phys. Rev. C **11**, 1203 (1975).
[26] W. D. Meyers and L. Schmidt, Nucl. Phys. **A310**, 61 (1983).
[27] S. Datz, H. F. Krause, C. R. Vane, H. Knudsen, P. Grafström, and R. H. Schuch, Phys. Rev. Lett. **77**, 2925 (1996).
[28] H. F. Krause, E. F. Deveney, N. L. Jones, C. R. Vane, S. Datz, H. Knudsen, P. Grafström, and R. Schuch, Nucl. Instrum. Methods Phys. Res., Sect. B **124**, 128 (1997).